Slow Photon Photocatalytic Enhancement using Titania Inverse Opal Photonic Crystals

V. Jovic, T. Söhnel, J.B. Metson and G.I.N. Waterhouse

Department of Chemistry, The University of Auckland, Auckland, New Zealand.

Titania inverse opal photonic crystals possessing photonic band gaps (PBGs) in the UV-Vis region were successfully fabricated using the colloidal crystal template approach. SEM, XRD, BET, Ti L-edge NEXAFS and optical measurements revealed these materials possess a 3-dimensionally ordered macroporous (3DOM) structure comprising air spheres in a nanocrystalline anatase TiO_2 matrix. The photocatalytic performance of the titania inverse opals under UV irradiation was evaluated, and slow photon photocatalytic enhancement of ethanol decomposition was observed for a TiO_2 inverse opal with a PBG at 344 nm.

1. Introduction

Photonic crystals are highly ordered materials that possess a periodically modulated refractive index in one, two or three dimensions, with periods typically on the length scale of visible light [1, 2]. Periodicity causes incoherent Bragg diffraction from lattice planes resulting in the creation of a photonic band gap (PBG), a narrow range of frequencies for which light propagation in the photonic crystal are forbidden. Opals and inverse opals (IO's) are important classes of photonic crystals. Opals comprise a *face-centered cubic* (*fcc*) arrangement of monodisperse solid spheres (ϕ_{solid} = 74%, ϕ_{void} = 26%), whereas inverse opals comprise a *fcc* arrangement of air spheres in a solid matrix (ϕ_{solid} < 26%, ϕ_{void} > 74%). The optical properties of opal and inverse opal photonic crystals can be described by the modified Bragg's Law expression below:

$$\lambda_{\max} = 1.633 D \sqrt{n_{avg}^2 - \sin^2 \theta}$$

where λ_{max} is the PBG position (in nm) for first order Bragg diffraction on *fcc*(111) planes, D is the sphere diameter (in nm), n_{avg} is the average refractive index of the photonic crystal and θ is the incident angle of light with respect to the surface normal of *fcc*(111) planes [3, 4]. At the edges of the PBG, light travels with a strongly reduced group velocity (v_g) resulting in the creation of slow photons [5, 6]. At the 'red edge' of the PBG, the incident light is localised on the dielectric material. If the 'red edge' of the PBG for titania inverse opals could be coupled to the electronic absorption band of TiO_2 (~388 nm), this should in theory enhance UV light absorption by the semiconductor, which in turn should enhance the photocatalytic activity of TiO_2 via increasing electron-hole pair formation. Inverse opal architectures have other desirable properties which make them ideal for catalytic and photocatalytic applications, such as large surface area and inherent macroporosity.

This project is aimed at the fabrication of TiO_2 inverse opal thin films and powders via the 'bottom up' colloidal crystal template approach. Here, the structural, optical and photocatalytic properties of a series of titania inverse opal photonic crystals are reported. The photocatalytic activities of the samples under UV irradiation have been evaluated against the photooxidation of gas phase ethanol.

2. Experimental

Batches of monodisperse PMMA colloids with diameters in the range 175-450 nm were synthesized by the free-radical-initiated emulsion polymerization of methyl methacrylate (MMA) [3, 7]. The PMMA suspensions were then transferred to 50 mL polypropylene centrifuge tubes and centrifuged at 1500 rpm for 24 h to form 3-dimensional PMMA colloidal crystals (synthetic opals). After centrifugation, the supernatant was decanted off and the PMMA colloidal crystal templates were dried in air for 3 weeks.

PMMA colloidal crystal thin films were fabricated on glass microscope slides using a flow controlled vertical deposition method [3, 8]. A PMMA colloid suspension (200 mL, 5wt % PMMA in H_2O) was poured into a 200 mL Duran glass petri dish. Glass microscope slides were vertically immersed in the PMMA colloidal suspension. A peristaltic pump, operating at a speed of 0.2 $mLmin^{-1}$, was used to slowly pump out the PMMA colloidal suspension. As the meniscus moved down the glass slide, a colloidal crystal thin film self-assembled at the falling meniscus with an *fcc* (111) plane parallel to the glass substrate.

TiO_2 inverse opal powders and thin films were prepared by the colloidal crystal template technique [3]. A titania sol was prepared by mixing ethanol (25 mL), titanium(IV) propoxide (25 mL), HCl (5 mL) and milli-Q water (10 mL). The titania sol was then applied drop-wise over the lightly crushed colloidal crystal template in a Buchner funnel under a strong vacuum. The infiltrated templates were left to hydrolyze in air at room temperature for 24 h, then carefully calcined at 300°C (2 h), then 400ºC (2 h), to remove the PMMA template and crystallize the TiO_2 network, respectively. Titania inverse opal thin films were prepared by diluting the titania sol 10-fold with ethanol and infiltrating the PMMA colloidal crystal thin films using capillary action.

3. Results

SEM micrographs of PMMA colloidal crystal templates of two different sizes (Samples 2 and 6) can be seen in Figure 1 (i) and (ii) below. The corresponding TiO_2 inverse opals are shown in Figures (iii) and (iv). From the SEM micrographs, sphere sizes were determined to be 215 and 452 nm, respectively. The corresponding inverse opal pore sizes calculated from these micrographs were 188 and 355 nm, respectively.

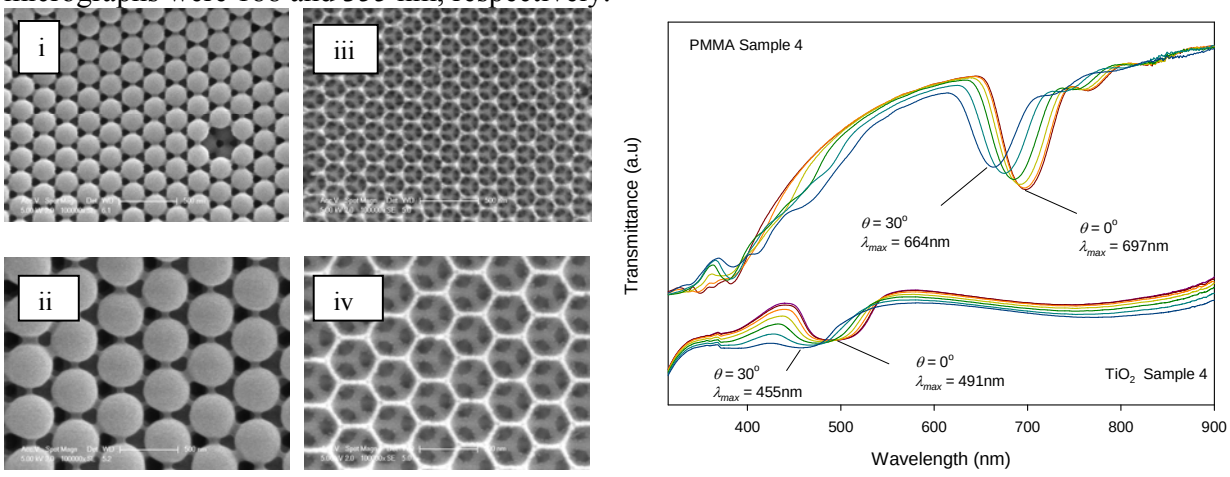

Figure 1(i) and (ii) show SEM micrographs for PMMA colloidal crystals of two different sizes. (iii) and (iv) show the corresponding TiO_2 inverse opals fabricated from the PMMA templates. The right panel shows UV-Visible transmission spectra for a PMMA colloidal crystal thin film (Sample 4) and its TiO_2 inverse opal replica. UV-Vis data were collected at angles of 0-30° with respect to the surface normal of the *fcc* (111) lattice planes.

Figure 1 (Right) shows UV-Vis transmittance spectra for a PMMA colloidal crystal and its titania inverse opal replica. At normal incidence ($\theta = 0^o$, i.e. along the [111] direction), the PMMA colloidal crystal exhibits a PBG at 697 nm, whereas the titania inverse opal shows a PBG at 491 nm, which reflects the lower solid volume fraction and lower average refractive index of the inverse opal. For both samples, the PBG shifts to shorter wavelengths as the incident angle of light with respect to the *fcc* (111) normal increases, in accordance with the modified Bragg's law given in the introduction. The PMMA colloidal crystals fabricated in this work showed PBGs at 396, 488 604, 697, 818 and 974 nm. The corresponding inverse opals had PBGs at <300, 344, 417, 491, 568 and 692 nm, respectively.

Powder XRD diffraction (Figure 2 Left) revealed that the titania inverse opals were composed of anatase nanoparticles of crystallite size ~11-16 nm. No rutile or brookite diffraction peaks were identified. Line broadening observed for the TiO_2 IO's confirmed the presence of nanocrystalline TiO_2 particles. Ti L-edge NEXAFS obtained at the Australian synchrotron presented in Figure 2 (Right) show characteristic L_3 and L_2 edge features which arise from the 2 $p_{3/2} \rightarrow$ 3d and 2 $p_{1/2} \rightarrow$ 3d electronic transitions of the octahedrally coordinated Ti^{4+} ion in anatase [9]. It is worth noting that the various TiO_2 polymorphs can be readily distinguished by NEXAFS but not by XPS.

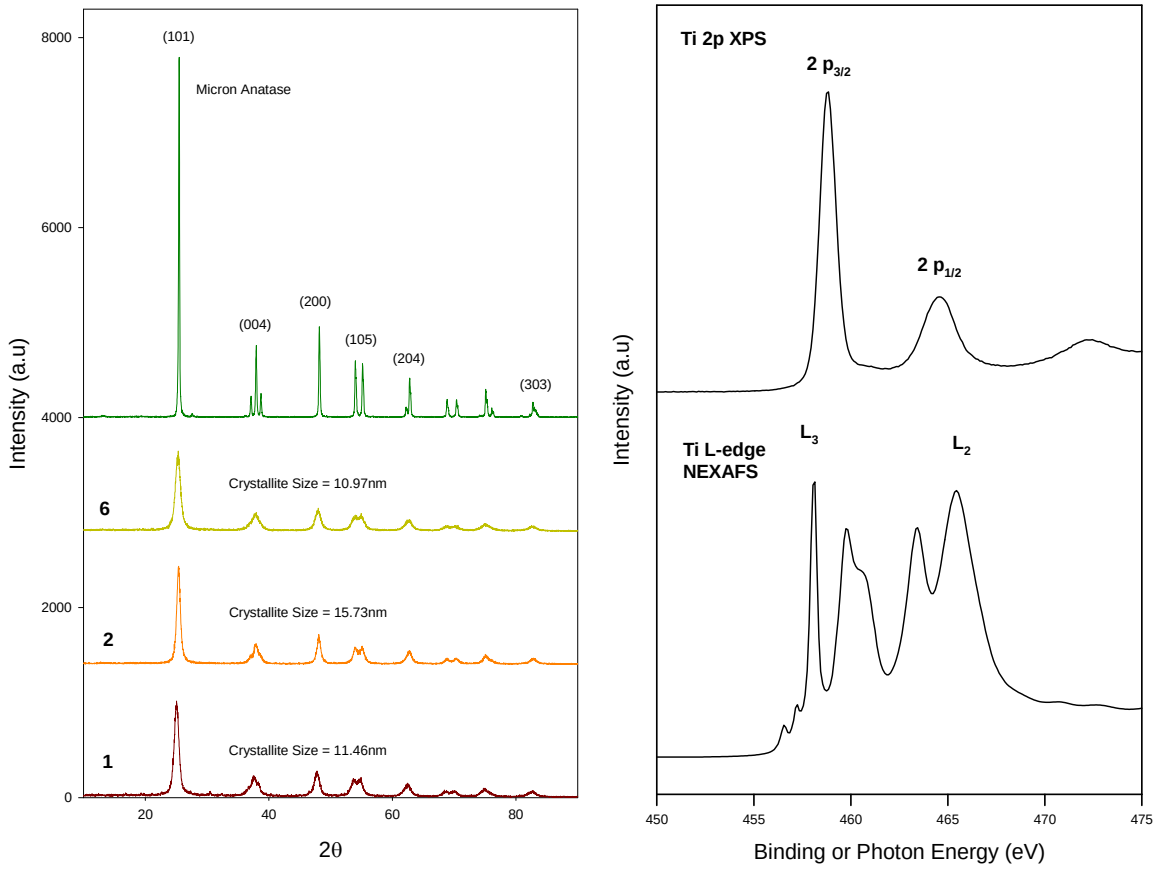

Figure 2 Left: Powder X-ray diffraction patterns for several TiO_2 inverse opal powders and a micron sized anatase TiO_2 powder. Right: Ti 2p XPS and Ti L-edge NEXAFS for a TiO_2 inverse opal.

The gas phase photo-oxidation of ethanol over the titania samples obeyed first order kinetics. The photocatalytic data is summarised in Table 1 below. The results show that Sample 2, which had a PBG at 344 nm, showed the highest rate constant (1.48×10^{-3} s^{-1}) amongst the photocatalysts tested. In this sample, the red edge of the PBG overlaps with the electronic absorption edge of TiO_2 (388 nm, ~3.2 eV). The low surface area anatase reference powder had the lowest rate constant (4.49×10^{-4} s^{-1}). The high surface area sample had a rate constant similar to Sample 1, a titania inverse opal operating outside the 'slow photon' regime. When the rate constants were normalized with respect to surface area, Sample 2 maintained the highest rate constant over the inverse opal samples (1.44×10^{-3} $s^{-1}m^{-2}$), confirming that slow photon photocatalytic enhancement, caused by overlap of the electronic absorption edge and red edge of the PBG, enhanced the rate constant.

Table 1. Summarized photocatalytic activity data for TiO_2 inverse opal powders and several anatase reference powders. The photocatalytic activities of the samples were evaluated under UV irradiation against the photodecomposition of gaseous ethanol.

Sample	PBG position (nm)	Area (m^2g^{-1})	Rate constant, k'(s^{-1})	Raw Enhancement factor	Normalized rate constant k'$_N$ ($s^{-1}m^{-2}$)	Enhancement factor
TiO_2 IO #1	<300.00	74.1	1.22×10^{-3}	1.51	1.09×10^{-3}	1.07
TiO_2 IO #2	344.95	68.9	1.48×10^{-3}	1.83	1.44×10^{-3}	1.41
TiO_2 IO #4	491.40	61.9	1.03×10^{-3}	1.28	1.11×10^{-3}	1.09
TiO_2 IO #6	568.20	52.7	8.07×10^{-4}	1	1.02×10^{-3}	1
HSA anatase	-	108.3	1.12×10^{-3}	1.52	7.57×10^{-4}	-
LSA anatase	-	10.4	4.49×10^{-4}	0.56	2.89×10^{-3}	-

Normalized rate constant k'$_N$($s^{-1}m^{-2}$) with respect to area. HSA; high surface area. LSA; low surface area.

Acknowledgements
The authors would like to thank Bruce Cowie for his assistance at the SXR beamline of the Australian Synchrotron and the New Zealand Synchrotron Ltd. for financial assistance.

References

[1] Yablonovitch E 1993 *Opt. Soc. Am. B.* **10** 283
[2] Yablonovitch E and Gmitter T J 1989 *Phys. Rev. Lett.* **18** 1950
[3] Schroden R C, Al-Daous M, Blanford C F and Stein A 2002 *Chem. Mater*. **14** 3305
[4] Waterhouse G I N, Metson J B, Idriss H and Sun-Waterhouse D 2008 *Chem. Mater*. **20** 1183
[5] Chen J I L and Ozin G A 2009 *J. Mater. Chem* **19** 2675
[6] Chen J I L, von Freymann G, Choi S Y, Kitaev V and Ozin G A 2008 *J. Mater. Chem*. **18** 369
[7] Waterhouse G I N and Waterland M W 2007 *Polyhedron* **26** 356
[8] Zhou Z and Zhao X S 2004 *Langmuir* **20** 1524
[9] Stewart S J, Fernandez-Garcia M, Belver C, Mun B S and Requejo F G 2006 *J. Phys. Chem. B* **110** 16482